Controlled mechanical fracture for fabricating microchannels with various size gradients†

Hong-Nam Kim, Sung-Hoon Lee and Kahp-Yang Suh*

Received 5th August 2010, Accepted 15th October 2010
DOI: 10.1039/c0lc00277a

We present a simple method to generate cracks with controllable size (depth and width) and space gradients using deep surface oxidation and anisotropic mechanical stretching. To generate a thick oxidation layer (<~7 μm), a polydimethylsiloxane (PDMS) slab of uniform or varying thickness was exposed to UV/ozone for less than 30 min in the UV-C wavelength including wavelengths of 185 and 254 nm. Subsequently, the PDMS slab was wrapped on a cylindrical support (radius: 11 mm) to apply a uniform bending strain (<21%), resulting in equally separated, anisotropic cracks over a large area. By modulating initial oxidation depth and applied bending stress, cracks of varying sizes and spaces were formed on a single PDMS slab. Furthermore, multiple, sequential cracks were generated by increasing the strain in a step-wise fashion and multi-directional cracks by applying the strain with an orientation angle. Finally, size and space-varying cracks were formed between two adjacent large channels in an interconnected format by selective masking and irreversible bonding.

1. Introduction

Cracks exist in various forms in nature and are generally conceived as an undesirable phenomenon, causing fracture of structures, breakdown of devices and collapse of buildings. Recently, a large number of studies have been carried out experimentally[1–6] and theoretically,[7–14] to generate and propagate cracks in a controlled fashion. Following the pioneering works by Takayama and coworkers,[1,2] it is now possible to generate controlled cracks on soft materials (*e.g.*, PDMS) *via* oxygen plasma treatment, which can be further utilized for microfluidic applications with the help of polymer replication techniques and irreversible bonding on glass substrate. Such geometry-controllable cracks would provide a cost-effective, low-expertise route to forming various micro- and nanoscale structures and channels.

Cracks result from a strain energy release process that is caused by mechanical fracture of a thin brittle layer bonded to another material. To emulate such a condition, PDMS has been widely used since it has relatively low elastic modulus (~1.8 MPa) and the top layer can be readily modified by deposition of a rigid material[15–22] or surface oxidation such as oxygen plasma[23–25] and UV/ozone treatment.[26–29] Although both approaches can produce a thin brittle layer on soft, rubbery PDMS polymer, the latter provides a better way of constructing monolithic dual (composition) layers without interfacial failure or thin film instability. It is noted that the two surface oxidation methods give different thicknesses of silicon oxides (SiO_x). For example, it has been shown that nanoscale cracks are formed (depth < 100 nm) on a thin brittle layer (<200 nm thickness) within 3 min of treatment for oxygen plasma treatment (shallow oxidation), which has been used for a variety of applications including trapping nanoparticles,[1] DNA manipulation[1] and cell-elongation.[2] In contrast, a significantly large portion of the top surface can be oxidized within 30 min of treatment for UV/ozone treatment (deep oxidation), resulting in a deeper oxidized layer up to ~14 μm.[30]

Under appropriate conditions, the surface oxidation can also lead to the formation of wrinkles ("buckling"),[31,32] which has been applied to microfluidic particle sieving system[33] and protein preconcentration[34] utilizing wrinkled nanochannels or flexible electronic devices.[15,18,21] Although cracks and wrinkles have some similarities, they are different in several aspects. First, cracks are generated as a consequence of mechanical fracture while wrinkles are induced by thin film instability. Therefore, the inner soft material could be exposed for cracks, which is not the case for wrinkling. Second, cracks are discrete and not connected to adjacent ones, while wrinkles are continuous. The spacing between cracks is typically ~10 times larger than the depth and width of the wrinkles. Third, secondary or tertiary cracks can be generated on pre-formed ones with application of an additional stress, resulting in a continuous path at the intersections. Although hierarchical wrinkles can be generated by controlled buckling,[33] secondary or tertiary wrinkles are generally different from initial ones in views of morphology and characteristic dimension and thus would not be suitable for use as a flow channel.

In this study, we report a simple, yet robust method for fabricating cracks with varying dimensions by employing deep surface oxidation of UV/ozone treatment at ambient conditions and anisotropic stretching by wrapping on a cylindrical support. We were motivated by the fact that previous experiments have mostly involved the formation of single scale cracks with less controllability over size and separation of cracks. In this method, cracks of various size (depth and width) and space gradients were

School of Mechanical and Aerospace Engineering, Seoul National University, Seoul, 151-742, Republic of Korea. E-mail: sky4u@snu.ac.kr

† Electronic supplementary information (ESI) available: Examples of sequential crack generation and masking-direction dependent crack generation, and a large-area photography of cracked PDMS slab are included. Also, AFM images before and after UV/Ozone treatment as well as after cracking are shown for comparison. See DOI: 10.1039/c0lc00277a

generated by independent control of initial oxidation thickness and applied bending stress. As described shortly, the thickness distribution of the oxidized layer determines the size of cracks, whereas the stress distribution the separation of cracks. By single or multiple controls of these two conditions, one can create distinctly observable cracks with specific size and space gradients, which can be directly used for fabricating microchannels of various dimensions.

2. Experimental

PDMS slab fabrication

PDMS slabs were prepared by curing PDMS pre-polymer (Sylgard 184 Silicon elastomer, Dow corning) on a flat or an inclined Petri dish with an inclination angle of 20°. To cure the PDMS pre-polymer, a mixture of 10 : 1 silicon elastomer and the crosslinker was poured onto the Petri dish and placed in an oven at 70 °C for 1.5 h. The PDMS slab was then peeled off and cut prior to use. The cross-section of the PDMS slabs used in the experiment was rectangular (length: 3.0 cm, height: 0.5 cm) or triangular (length: 3.0 cm, height: 1.0 cm).

Crack generation

The surface of PDMS slab was oxidized with UV/ozone treatment system (Yuil Ultra Violet System, Korea) for a period of time (<30 min) under controlled distance. For uniform height and height-varying treatment conditions, the inclined angle was fixed at 0° and 20°, respectively. The distance from UV lamp at the middle location was fixed at 5 cm. In the case of uniform height, the distance from UV lamp was constant at 5 cm. The dose of UV/ozone was 15–20 mW cm^{-2} (when measured within 10 mm distance) in UV-C wavelength including wavelengths of 185 and 254 nm. After UV irradiation, cracks were generated by wrapping the PDMS slab on a cylinder support whose radius was 11 mm.

Data acquisition

Usually 50–100 of cracks were generated on 3 cm long PDMS substrates. To measure the crack size and spacing, the samples were cut equally into four pieces in which roughly 10–25 cracks existed. Then, all cracks were examined on each sample piece (some non-fully propagated cracks were excluded), and the measured values were averaged. For statistical significance, each run was repeated ~50 times.

Crack replication and visualization with a fluorescent dye

Cracks are usually prone to clogging as time goes by. To utilize permanent deformation of cracks, replica molding technique[1,2,35,36] was used. Cracks were replicated from the strained PDMS substrate which was attached onto a curved plane (radius of curvature: 5 cm) with a double-sided tape. Subsequently, UV-curable polyurethane acrylate (PUA) precursor was drop-dispensed on the curved substrate and brought into contact with a 100 μm thick polyethylene terephthalate (PET) film as a backing plane. After curing, a negative PUA replica was formed on the PET film with the pre-defined curvature. Since the PUA replica is sufficiently rigid and flexible, it was easily flattened and attached onto a Petri dish with a double-sided tape. Finally, the PDMS precursor was poured and replicated in the same manner. By doing this, the original cracks were restored without shape change and an irreversible bonding of the cracks to glass substrate was possible for channel fabrication. To visualize crack generation and show abilities for microfluidic applications, a dilute solution of Rhodamine B dye (0.05 wt%, Sigma, St Louis, MO) in deionized water was introduced inside the cracks after PDMS bonding. The fluorescent images were taken using Olympus IX71 microscope (Olympus, Japan).

Scanning electron microscopy

High-resolution scanning electron microscopy (SEM) images were obtained using HITACHI S-4800 microscope (Hitachi, Japan) operating at an accelerating voltage of 10 kV. To avoid charging effects, PDMS was sputter coated with Pt to the thickness of 5 nm prior to measurements.

Fabrication of microchannels

Microchannels of 50 μm width and 50 μm height were fabricated by replica molding technique with PDMS. These parallel microchannels were separated by 500 μm. The replicated PDMS channel was treated with UV/ozone for 30 min after selectively masking the strip region bridging two adjacent microchannels. By wrapping on a cylindrical support (radius: 11 mm), cracks of varying size gradients were generated on the exposed region. For use as flow channels, the UV/ozone treated PDMS channel was first replicated with PUA and then with PDMS. The double-replicated PDMS was punched to make inlet and outlet reservoirs and finally irreversibly bonded to slide glass after oxygen plasma treatment.

3. Results and discussion

Fig. 1 shows a schematic illustration of the experimental procedure. As shown in Fig. 1(a), a thin PDMS slab of equal thickness or varying thickness was conformably wrapped around a cylindrical support (diameter: 11 mm), after UV/ozone treatment for a period of time (<30 min) at ambient conditions. Upon stretching, the oxidized upper layer of PDMS slab is subject to a tensile stress, so that cracks are spontaneously generated when the applied strain exceeds a critical value ε_c. During the UV/ozone treatment, various chemical reactions are known to occur in steps.[26] First, UV irradiation with shorter wavelength (~185 nm) generates ozone from atmospheric oxygen, which is subsequently photo-dissociated into molecular oxygen and atomic oxygen with the aid of UV light of longer wavelength (~254 nm). Then, the produced atomic oxygen reacts with CH_3– groups, which are ultimately removed in the form of volatile products such as carbon dioxide and water, leaving behind a thin brittle film of SiO_x. The thin oxidized layer thus formed has higher elastic modulus compared to that of untreated PDMS block, forming a monolithic composition layer (brittle oxidized layer + elastic substrate). In the experiment, large, visible cracks were not self-generated if the treatment time was less than ~30 min. If the treatment time was longer than ~30 min,

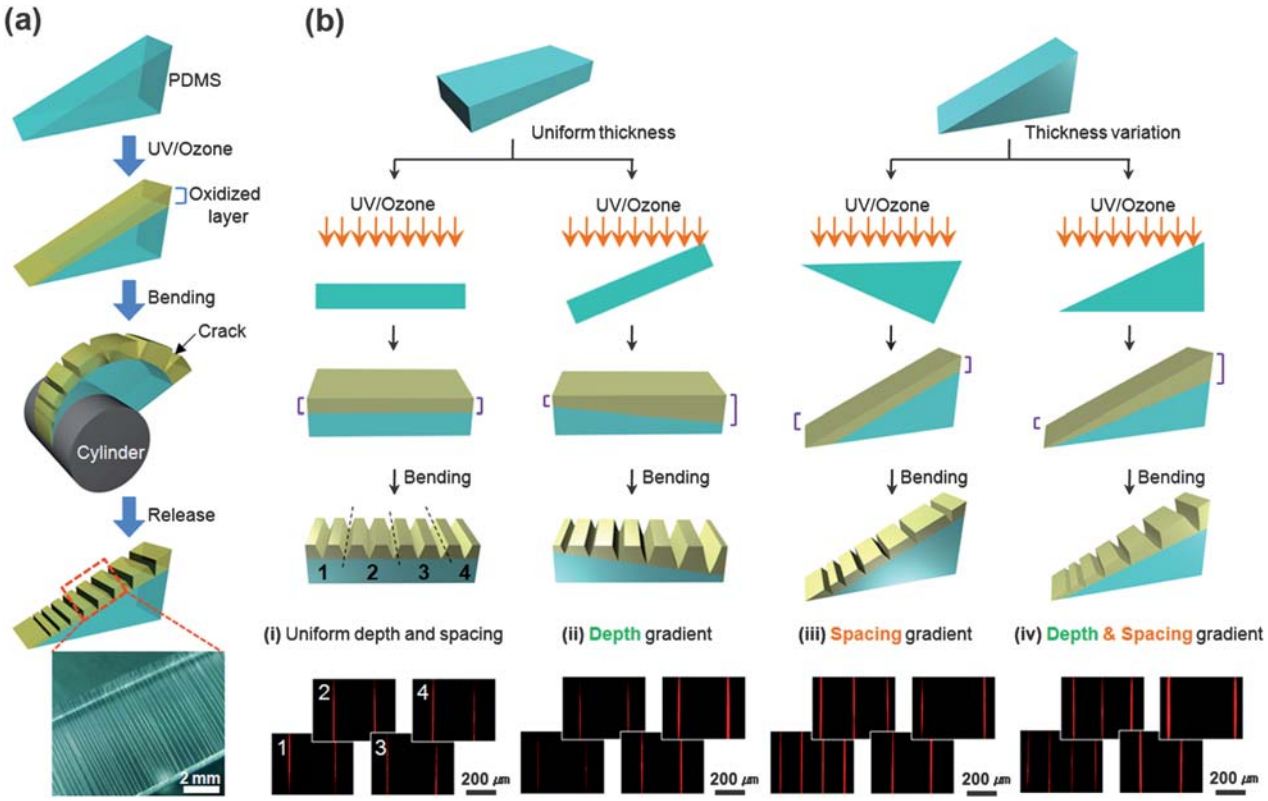

Fig. 1 (a) Schematic illustration of generating cracks with various dimensions. A PDMS slab of uniform or varying thickness was wrapped on a cylindrical support to apply a certain tensile stress. A photograph for large-area fabrication is shown on the bottom. (b) Four controlled experiments with a uniform or a thickness-varying PDMS slab. Depending on the distribution of initial oxidation thickness and applied bending stress, cracks of size and/or space gradients were generated. Representative experimental results were displayed with a red-fluorescent dye for four consecutive regions from the sample (see Experimental section).

randomly distributed cracks were spontaneously generated without additional mechanical stretching.

Fig. 1(b) shows four controlled experiments with an equal-thickness (cross-section: rectangular) or a thickness-varying (cross-section: triangular) PDMS slab to create cracks of varying sizes and spaces. As shown, two parameters were independently controlled: thickness of the PDMS slab (uniform or linear with an inclination angle of 20°) and thickness of the initial oxidized layer (uniform or linear with an inclination angle of 20°). With an inclination angle, the distance from UV lamp is modified along the surface, which in turn changes the dose of UV irradiation and the oxidation thickness, accordingly. For an equal-thickness PDMS slab, the slab is subject to a uniform tensile stress, thereby generating equally separated cracks (i). For an equal-thickness PDMS slab with a linearly increasing oxidation thickness profile, the same tensile stress is applied and renders equally separated cracks of "varying depths and widths" (ii). Similarly, with a thickness-varying PDMS slab, the applied tensile stress is linearly increasing with the decrease of the slab thickness, producing a smaller space on the highly loaded region (thinner part) and a larger space on the less loaded region (thicker part). At the same time, the size of cracks can be controlled by using a uniform (iii) or a linearly increasing oxidation thickness profile (iv), as with the cases of (i) and (ii). It is noted that, from the fracture mechanics point of view, the spacing would increase with increasing the crack depth if the stress is uniform (case 2).[13] As shown in Fig. 2, the depth varies from 3.5 μm (region 1) to 5.0 μm (region 4) at an inclination of 20°, whose difference seems not high enough to observe such depth-related effects.

To demonstrate the influence of different geometric conditions, the experiments were classified into four groups. Fig. 2 shows representative SEM images of cracks under four different cases along with corresponding plots for the variation of crack dimension. For each figure set, the upper and lower parts, respectively, indicate a tilted and a cross-sectional view of the cracks from four consecutive regions from the sample. As can be seen from the figure, various size and space gradients were generated with respect to the use of different geometric condition. According to the SEM images, each crack can be viewed as a crater of parabolic shape, as opposed to sharp cracks (grooves) observed in previous studies.[7] It is intriguing that such gradient patterns can be fabricated in one-step without the use of sequential multi-step photolithography[37,38] or photolithography with gray-scale mask.[39–41]

To elaborate on controlled generation and propagation of cracks, we examine the oxidation depth as a function of time. In view of similarity to traditional oxidation process of silicon wafer in a furnace, the well-known Deal–Grove model[42] can be used here to describe the oxidation thickness with the UV/ozone exposure time. The model predicts that the thickness of oxidation layer would increase in proportional to $t^{0.5}$ (t is the exposure time), which is in good agreement with the data shown in

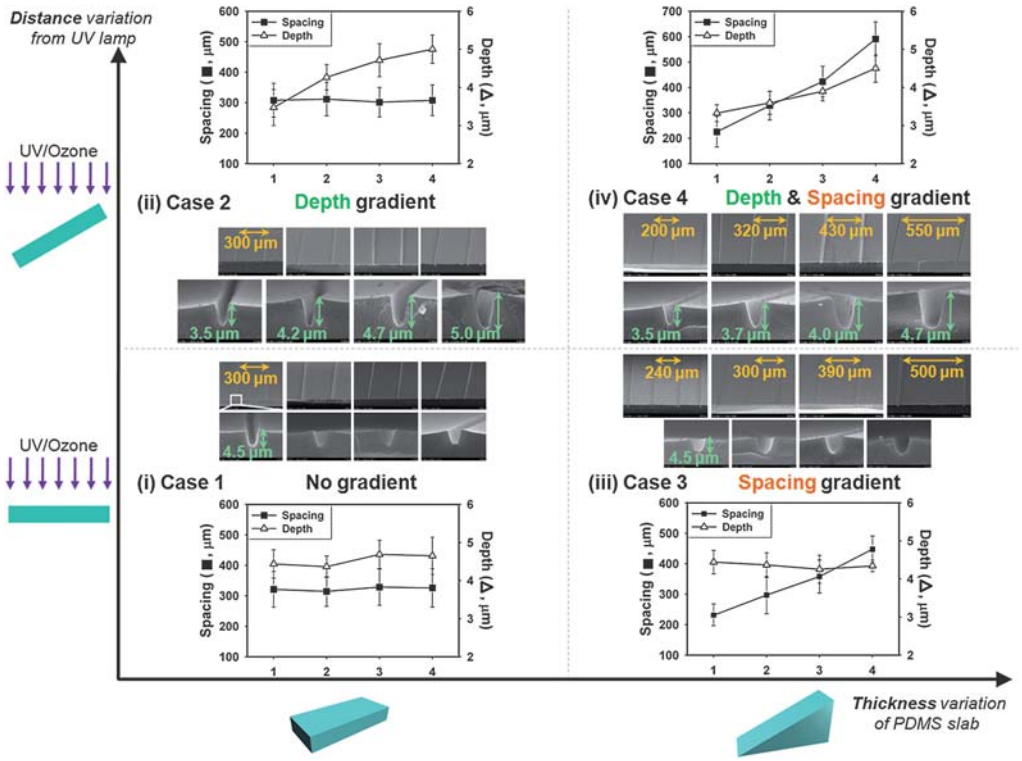

Fig. 2 A structure map for the generation of cracks with various dimensions by controlling the thickness of PDMS slab and distance from UV lamp. For each condition, representative SEM images (titled and cross-sectional view) as well as plots for the variation of crack dimension are shown.

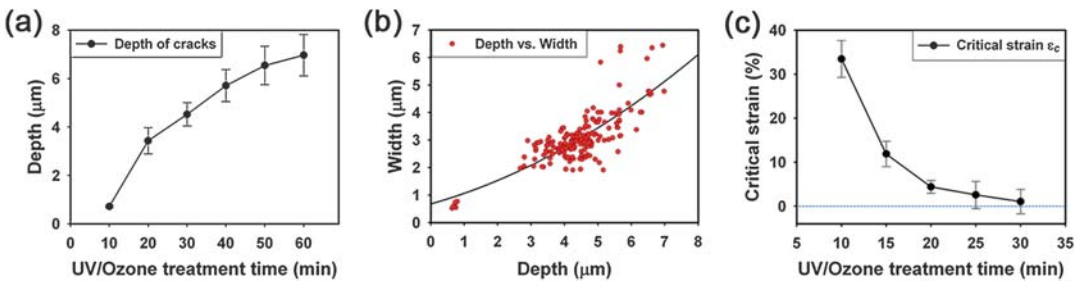

Fig. 3 (a) Plot of the oxidation depth as a function of time. Note that a parabolic increase was observed, in accord with the Deal–Grove model. (b) The relation between width and depth of cracks for three UV/ozone treatment times of 10, 20 and 30 min. (c) The change of critical strain with exposure time. For the experiment, PDMS slabs of uniform thickness (5 mm) and uniform distance from UV lamp (5 cm) were used (case 1 in Fig. 2).

Fig. 3(a). Also, it was observed that the depth of cracks was primarily determined by the exposure time and then the width was proportionally increased (not linear) with the increase of the depth [Fig. 3(b)]. In order to generate uniform cracks, it is important to understand the critical strain ε_c that is needed for the onset of cracks. Fig. 3(c) demonstrates that ε_c is highly affected by the UV/ozone treatment time, such that ε_c decreases dramatically as the treatment time increases. For example, ε_c was 33% for 10 min treatment, which was sharply reduced to 1% for 30 min exposure. When the exposure time was larger than 30 min, randomly distributed cracks started to appear as a result of built-in residual stress.

As is well known, cracking is an inherently stochastic phenomenon, as initial defects or imperfections in SiO_x layer can act as crack initiators. For this reason, crack generation is relatively random at initial stage compared to middle or final stage. Nahta and Moran reported[43] that there is a minimum crack spacing at a given stress that is associated with the applied stress. This means that the spacing between cracks should be larger than the minimum separation irrespectively of multiple crack formations. As a consequence, the spacing would become more uniform as the cracks are more densely populated, in comparison to early stage, randomly generated cracks with large deviation. This narrowing down process of randomness is well presented in a sequential crack formation where the strain was increased in a step-wise fashion from 1% to 8% (see ESI, S1†). In our experiment, we applied a high bending stress in order to generate nearly stress-free, uniformly separated cracks. Moreover, the bending stress was applied in an anisotropic fashion with both ends acting as nodes, which further helped forming well-aligned, highly uniform cracks along the surface.

The generation and propagation of directional, anisotropic cracks can also be performed several times with an orientation angle. Fig. 4 shows multi-directional crack generation with

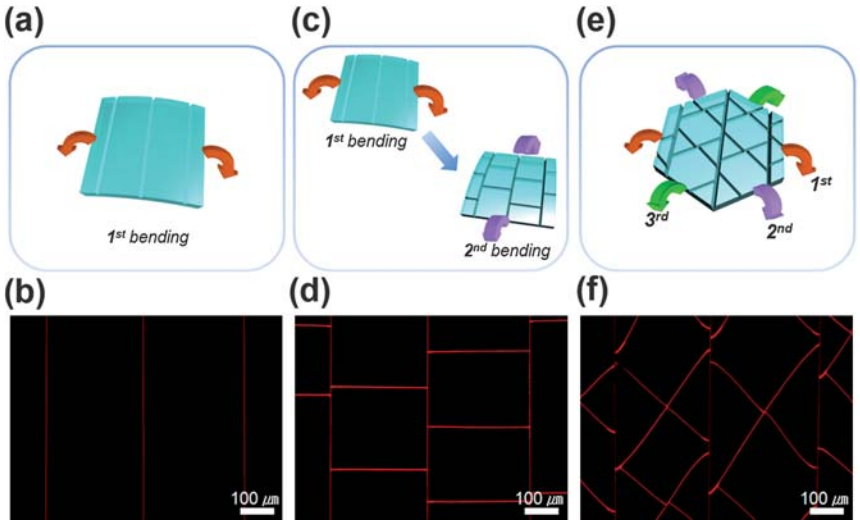

Fig. 4 Schematic illustration (a, c, and e) and corresponding results (b, d, and f) for the generation of multiple cracks with an orientation angle. (a and b) Parallel, equally separated cracks by single bending at 15% strain. (c and d) Bi-directional, mesh-type cracks by sequential application of 17% strain at 90° rotation angle. (e and f) Tri-directional cracks with double applications of 21% strain at 60° rotation angle with respect to each other. Cracks propagate with curved trajectory to meet at right angle in the intersection.

respect to the direction of applied strain. Parallel cracks were first generated with a unidirectional strain at 15% [Fig. 4(a) and (b)]. Then, bi-directional, mesh-type cracks were generated by applying a strain orthogonally at 17% [Fig. 4(c) and (d)]. Interestingly, the secondary cracks could not propagate across the boundaries of the first generated ones, suggesting that the pre-formed cracks can act as a propagation barrier. In addition, tri-directional cracks were generated by applying a strain at 21% two times with an angle of 60° with respect to each other [Fig. 4(e) and (f)]. Although multiple cracks were formed with an apparent orientation angle, the cracks always merged at 90° at the intersections, which agrees with an earlier theoretical study.[10] Compared to the unidirectional cracks depicted in Fig. 4(a) and (b), bi-directional and tri-directional cracks require a higher strain energy since the previously generated cracks (unidirectional cracks) release the strain energy by widening their width. In this experiment, for visualization purpose, a red fluorescent dye (Rhodamine B) was introduced inside the cracks after irreversible bonding of a double-replicated PDMS replica onto glass substrate (see Experimental details).

The generation of cracks was also strongly affected by the masking direction. For example, aligned or ladder-like cracks (4.5 μm depth, 3.0 μm width) were formed along the exposed area, in which the mask had been placed at 90° and 45° with respect to the direction of channels (see ESI, S2†). Similar to the previous findings in Fig. 4, cracks did not propagate across the initial microchannels and were independently generated without any interaction with the neighboring ones. These results suggest that each crack is governed by its own boundary condition where the initial microchannels can act as nodes, confining each crack within the surface-modified strip region and merging at 90° at the intersections. The depth of microchannels was 105 μm which was more than 15 times deeper than that of cracks. Interestingly, the location of the cracks was determined by the demarcation between the masked and unmasked regions (white dotted lines in Fig. S2†), so that the cracks were formed at the middle of the exposed rod regions.

By utilizing selective masking and irreversible bonding, one can fabricate small micro- and nanochannels of various size gradients that can bridge two large microchannels. A schematic diagram of the experimental procedure is shown in Fig. 5(a) along with an illustration of the chip design (b) and representative fabrication results (c). Here, two 50 μm channels separated by 500 μm are connected by size-varying cracks. To generate cracks of varying size gradients, a thickness varying PDMS was

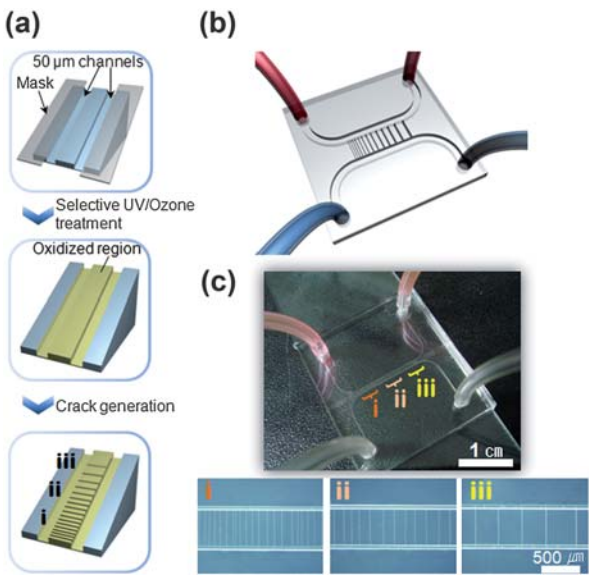

Fig. 5 Fabrication of microchannels of varying size gradients. (a) With the method described in Fig. 1, a portion of the channel was exposed to UV/ozone for selective surface modification. (b) Schematic illustration of the microfluidic chip with depth and space gradient. Two 50 μm channels spaced 500 μm apart are connected *via* cracks. (c) Photograph and microscopic images showing the microchannels fabricated after channel bonding. As shown, the three regions denoted as (i), (ii) and (iii) show different crack dimensions in terms of depth, width and spacing.

exposed to UV/ozone for 30 min. Then, the surface-modified PDMS channel was double-replicated with PUA and PDMS, and subsequently bonded to glass substrate.

As shown in Fig. 5(c), the bridging channels were neatly formed within the exposed strip area without crossover or penetration into the existing channels. The size of cracks ranged from 700 nm to 7 μm with the corresponding variation of depth and space (see Fig. 3), which can allow for testing the effect of various channel dimensions in a single experiment. Moreover, these channels would be particularly useful for various cell studies such as cell communication in co-culture format[44] and controlled neuronal growth.[45]

4. Conclusions

We have presented a simple and highly reproducible method to generate cracks of varying dimensions in terms of size (depth and width) and space by directionally stretching a surface-oxidized PDMS slab on a cylindrical support. The UV/ozone treatment led to a deep, brittle oxidation layer (<~7 μm) with a built-in residual stress and an external bending stress onto the pre-strained layer gave birth to directional cracks with distinct periodicity, with the applied strain being larger than the critical value. The control of size and space gradients was achieved by independently modulating the thickness of PDMS slab and distance from UV source. Furthermore, multiple, sequential generation of cracks was demonstrated by applying multiple strains with an orientation angle. Finally, the fabrication of interconnected microchannels with varying size gradients was demonstrated by utilizing selective surface masking and irreversible channel bonding. These methods offer a simple, low expertise route to fabricating well-defined channels with various dimensions without resorting to other complicated or expensive methods.

Acknowledgements

This work was supported by World Class University program on multiscale mechanical design (R31-2008-000-10083-0), Korea Research Foundation Grant (MOEHRD) (KRFJ03003), and Basic Science Research Program through the National Research Foundation grant (2010-0027955) funded by the Ministry of Education, Science and Technology (MEST).

References

1 D. Huh, K. L. Mills, X. Zhu, M. A. Burns, M. D. Thouless and S. Takayama, *Nat. Mater.*, 2007, **6**, 424–428.
2 X. Zhu, K. L. Mills, P. R. Peters, J. H. Bahng, E. H. Liu, J. Shim, K. Naruse, M. E. Csete, M. D. Thouless and S. Takayama, *Nat. Mater.*, 2005, **4**, 403–406.
3 L. M. Gao, E. T. Thostenson, Z. Zhang and T. W. Chou, *Adv. Funct. Mater.*, 2009, **19**, 123–130.
4 T. C. Lin, L. C. Huang, T. R. Chou and C. Y. Chao, *Soft Matter*, 2009, **5**, 3672–3676.
5 R. P. Wool, *Soft Matter*, 2008, **4**, 400–418.
6 K. L. Mills, D. Huh, S. Takayama and M. D. Thouless, *Lab Chip*, 2010, **10**, 1627–1630.
7 T. Y. Tsui, A. J. McKerrow and J. J. Vlassak, *J. Mater. Res.*, 2005, **20**, 2266–2273.
8 Z. C. Xia and J. W. Hutchinson, *J. Mech. Phys. Solids*, 2000, **48**, 1107–1131.
9 J. L. Beuth and N. W. Klingbeil, *J. Mech. Phys. Solids*, 1996, **44**, 1411–1428.
10 J. Liang, R. Huang, J. H. Prevost and Z. Suo, *Int. J. Solids Struct.*, 2003, **40**, 2343–2354.
11 L. Rey, N. Poisson, A. Maazouz and H. Sautereau, *J. Mater. Sci.*, 1999, **34**, 1775–1781.
12 V. B. Shenoy, A. F. Schwartzman and L. B. Freund, *Int. J. Fract.*, 2001, **109**, 29–45.
13 M. D. Thouless, E. Olsson and A. Gupta, *Acta Metall. Mater.*, 1992, **40**, 1287–1292.
14 R. Long and C. Y. Hui, *Soft Matter*, 2010, **6**, 1238–1245.
15 A. J. Baca, J. H. Ahn, Y. G. Sun, M. A. Meitl, E. Menard, H. S. Kim, W. M. Choi, D. H. Kim, Y. Huang and J. A. Rogers, *Angew. Chem., Int. Ed.*, 2008, **47**, 5524–5542.
16 C. M. Stafford, C. Harrison, K. L. Beers, A. Karim, E. J. Amis, M. R. Vanlandingham, H. C. Kim, W. Volksen, R. D. Miller and E. E. Simonyi, *Nat. Mater.*, 2004, **3**, 545–550.
17 S. P. Lacour, D. Chan, S. Wagner, T. Li and Z. G. Suo, *Appl. Phys. Lett.*, 2006, **88**, 204103.
18 D. Y. Khang, J. A. Rogers and H. H. Lee, *Adv. Funct. Mater.*, 2009, **19**, 1526–1536.
19 P. J. Yoo, K. Y. Suh, H. Kang and H. H. Lee, *Phys. Rev. Lett.*, 2004, **93**, 34301.
20 C. M. Stafford, B. D. Vogt, C. Harrison, D. Julthongpiput and R. Huang, *Macromolecules*, 2006, **39**, 5095–5099.
21 D. H. Kim, J. H. Ahn, W. M. Choi, H. S. Kim, T. H. Kim, J. Z. Song, Y. G. Y. Huang, Z. J. Liu, C. Lu and J. A. Rogers, *Science*, 2008, **320**, 507–511.
22 D. C. Hyun, G. D. Moon, E. C. Cho and U. Y. Jeong, *Adv. Funct. Mater.*, 2009, **19**, 2155–2162.
23 H. Hillborg, J. F. Ankner, U. W. Gedde, G. D. Smith, H. K. Yasuda and K. Wikström, *Polymer*, 2000, **41**, 6851–6863.
24 K. L. Mills, X. Zhu, S. Takayama and M. D. Thouless, *J. Mater. Res.*, 2008, **23**, 37–48.
25 P. Kim, R. Kwak, S. H. Lee and K. Y. Suh, *Adv. Mater.*, 2010, **22**, 2426–2429.
26 M. Ouyang, C. Yuan, R. J. Muisener, A. Boulares and J. T. Koberstein, *Chem. Mater.*, 2000, **12**, 1591–1596.
27 K. Efimenko, W. E. Wallace and J. Genzer, *J. Colloid Interface Sci.*, 2002, **254**, 306–315.
28 H. E. Jeong, M. K. Kwak and K. Y. Suh, *Langmuir*, 2010, **26**, 2223–2226.
29 C. J. Yu, C. Masarapu, J. P. Rong, B. Q. Wei and H. Q. Jiang, *Adv. Mater.*, 2009, **21**, 4793–4797.
30 Y. Berdichevsky, J. Khandurina, A. Guttman and Y. H. Lo, *Sens. Actuators, B*, 2004, **97**, 402–408.
31 J. Y. Chung, J. P. Youngblood and C. M. Stafford, *Soft Matter*, 2007, **3**, 1163–1169.
32 A. Chiche, C. M. Stafford and J. T. Cabral, *Soft Matter*, 2008, **4**, 2360–2364.
33 K. Efimenko, M. Rackaitis, E. Manias, A. Vaziri, L. Mahadevan and J. Genzer, *Nat. Mater.*, 2005, **4**, 293–297.
34 S. Chung, J. H. Lee, M. W. Moon, J. Han and R. D. Kamm, *Adv. Mater.*, 2008, **20**, 3011–3016.
35 T. I. Kim and K. Y. Suh, *Soft Matter*, 2009, **5**, 4131–4135.
36 M. K. Kwak, H. E. Jeong, T. I. Kim, H. Yoon and K. Y. Suh, *Soft Matter*, 2010, **6**, 1849–1857.
37 A. Mata, A. J. Fleischman and S. Roy, *J. Micromech. Microeng.*, 2006, **16**, 276–284.
38 C. Greiner, E. Arzt and A. del Campo, *Adv. Mater.*, 2009, **21**, 479–482.
39 H. Wu, T. W. Odom and G. M. Whitesides, *Anal. Chem.*, 2002, **74**, 3267–3273.
40 C. Chen, D. Hirdes and A. Folch, *Proc. Natl. Acad. Sci. U. S. A.*, 2003, **100**, 1499.
41 C. M. Waits, A. Modafe and R. Ghodssi, *J. Micromech. Microeng.*, 2003, **13**, 170–177.
42 S. M. Sze, *Semiconductor Devices: Physics and Technology*, Wiley India Pvt. Ltd., 2008.
43 R. Nahta and B. Moran, *Eng. Fract. Mech.*, 1995, **52**, 513–524.
44 D. Wright, B. Rajalingam, S. Selvarasah, M. R. Dokmeci and A. Khademhosseini, *Lab Chip*, 2007, **7**, 1272–1279.
45 A. M. Taylor, M. Blurton-Jones, S. W. Rhee, D. H. Cribbs, C. W. Cotman and N. L. Jeon, *Nat. Methods*, 2005, **2**, 599–605.

